JOURNAL OF MATERIALS SCIENCE 21 (1986) 475–487

# Superplastic deformation in Ti–4% Al–4% Mo–2% Sn–0.5% Si (IMI550)

JIMIN MA
*Institute of Aeronautical Materials, Beijing, People's Republic of China*
R. KENT, C. HAMMOND
*Department of Metallurgy, University of Leeds, UK*

The superplastic deformation properties, i.e. flow stresses and strain rate sensitivities, of the commercial alloy Ti–4% Al–4% Mo–2% Sn–0.5% Si (IMI550) have been assessed in the temperature range 805 to 915° C and for different initial microstructures. Fine grained $\alpha + \beta$ microstructures showed superplastic properties at temperatures above 850° C and grain coarsening, which led to increases in flow stresses and a reduction in superplastic properties, was only pronounced at the higher temperatures. In transformed $\beta$ microstructures the method of strain rate cycling led to a breakdown of the acicular $\alpha$ platelets and the development of an equiaxed $\alpha + \beta$ microstructure. At the same time the flow stresses at low strain rates decreased and the strain rate sensitivities increased. Light and electron microscopy showed that the $\beta$-phase became the continuous or matrix phase even at volume fractions below 50% (i.e. at the lower deformation temperatures) and that molybdenum segregation at the longitudinal interphase boundaries (parallel to the tensile axis) occurred. The results suggest that there is a strain distribution between the $\alpha$-phase and the $\beta$-phase, the $\beta$-phase effectively behaving as a deforming mantle around the $\alpha$ grains.

## 1. Introduction

The alloy IMI550 (Trade Mark, IMI Titanium Ltd) is a high strength ($\alpha + \beta$) titanium alloy with nominal chemical composition (wt %) Ti–4 Al–4 Mo–2 Sn–0.5 Si [1]. The aluminium, tin and silicon solid solution strengthen and stabilize the $\alpha$-phase and the molybdenum strengthens and stabilizes the $\beta$-phase and widens the ($\alpha + \beta$) phase field. The silicon may also provide a source of precipitation strengthening and grain refinement depending upon heat treatment. The alloy is produced in ($\alpha + \beta$) forged and rolled bar, plate or sheet forms and the recommended heat treatment is a 900° C anneal (in the $\alpha + \beta$ field) followed by a 500° C ageing treatment.

The microstructure consists of equiaxed $\alpha$ + (transformed) $\beta$ grains where the grain sizes, volume fractions and scale of the acicular $\alpha$ in the transformed $\beta$ grains are largely determined by variations in the thermochemical processing procedures, and to a much lesser extent upon variations in alloy chemistry.

In the sheet form the $\alpha$/transformed $\beta$ grain sizes are of the order 2 to 4 $\mu$m and recent work has shown [2] that it can be superplastically formed into complex shapes at temperatures as low as 850° C. However, the relationships between grain size and superplastic formability in sheet material and even the basic material properties such as the variations in strain rate sensitivity with temperature and strain rate and the effects of grain growth have not yet been established. This is in marked contrast to the situation which applies to the alloy Ti–6% Al–4% V (IMI318) which has been the subject of a large amount of research with respect to its superplastic properties in simple tension [3–6], biaxial tension (sheet forming) [7, 8] and compression (isothermal forging) [9, 10].

The present work was therefore undertaken in order to assess the superplastic properties (particularly strain rate sensitivities) of IMI550 over a range of temperatures and for different initial microstructures ranging from fine grained equiaxed ($\alpha + \beta$) to coarse transformed $\beta$ microstructures. The changes in microstructure which may occur during testing are also correlated with the changes in flow stresses and strain rate sensitivities.

Almost all theories of superplasticity involve (a) a description of grain switching/sliding processes, and (b) an analysis of the rate-controlling mechanisms for these processes. A generally widely accepted theory is that of Ashby and Verrall [11] who derived a constitutive equation based upon a grain switching mechanism which is rate-controlled at low strain rates by a combination of Herring–Nabarro and Coble diffusional creep processes (in which the characteristic diffusional path lengths are substantially smaller than the grain size) and at higher strain rates by dislocation climb-controlled creep processes. The constitutive equation also incorporates a threshhold or internal stress term which arises from the work required in changing the configuration of the grains during the grain switching process and the fluctuations in the length of grain boundary dislocations which occur as the grain boundaries act as sources and sinks for vacancies [12].

The Ashby–Verrall mechanism has been criticized

0022–2461/86 $03.00 + .12 

by Gifkins [13] who points out that as it is essentially a topologically two-dimensional model it does not predict the increase in surface area with strain, and by Springarn and Nix [14] who point out that the diffusion paths in the model need to be modified to account for the tractions across the grain boundaries. However, its main limitation is that it only describes the properties of single-phase materials and fails to account for the usual situation of two-phase materials in which the two phases may have substantially different diffusional properties. This is particularly the case in titanium alloys in which the $\beta$-phase is, at homologous temperatures above about 0.5, softer than the $\alpha$-phase by virtue of its "anomalously" high diffusional properties [15]. As shown by Springarn and Nix [14] in two-phase alloys, atoms in the faster diffusing ($\beta$) phase collect at the ($\alpha$) grain boundaries, "wedging" the $\alpha$ grains apart and replacing $\alpha$ grain boundaries with $\alpha/\beta$ interphase boundaries. In this way the $\beta$-phase becomes the connected or continous phase in the microstructure.

The main problem in describing the superplastic properties of such two-phase materials is in determining in what ways the separate properties of the two dissimilar phases should be combined. Two "laws of mixtures" equations have been advanced [16, 17]. In one limiting case, the "isostress" model, the stresses in the $\alpha$-phases and $\beta$-phases, are assumed to be constant resulting in differential strain rates between the phases. In the other limiting case, the "isostrain rate model", the strain rates in the $\alpha$-phases and $\beta$-phases are assumed to be constant, resulting in differences in the stresses between the two phases. The experimental evidence [18, 19] does not yet confirm the applicability of either model.

There is a further complication in assessing the superplastic properties of IMI550 in relation to the Ashby–Verrall mechanism which does not apply to Ti–6% Al–4% V. The diffusivity of vanadium in $\beta$ titanium is very close to that for titanium in $\beta$ titanium [15] and hence the $\beta$-phase in Ti–6% Al–4% V can be approximated to a single component phase with respect to its diffusional properties. This is not the case in IMI550 because molybdenum has a lower diffusivity – by about an order of magnitude in the temperature range of interest – than titanium in $\beta$-titanium. Hence solute segregation (to the longitudinal grain boundaries) and solute drag effects are likely to occur. The situation is in a sense the reverse of that which applies to Ti–6% Al–4% V in which small alloying additions of the fast diffusing alloying elements, cobalt, nickel or iron, have been added [18, 19] and in which solute segregation (to the transverse grain boundaries) has been detected [20].

## 2. Alloy and experimental procedure

The alloy was supplied as 27 mm diameter hot rolled bar, IMI Cast no. C5452 with chemical composition (wt %): Ti–4.01 Al–4.08 Mo–2.13 Sn–0.42 Si–0.04 Fe–0.03 C–0.185 O–0.015 H. The $\beta/(\alpha + \beta)$ transus temperature was 980 to 985° C. The bar was reduced to 16 mm diameter by hot rolling either in the $(\alpha + \beta)$ field or in the $\beta$ field, followed by air cooling from the

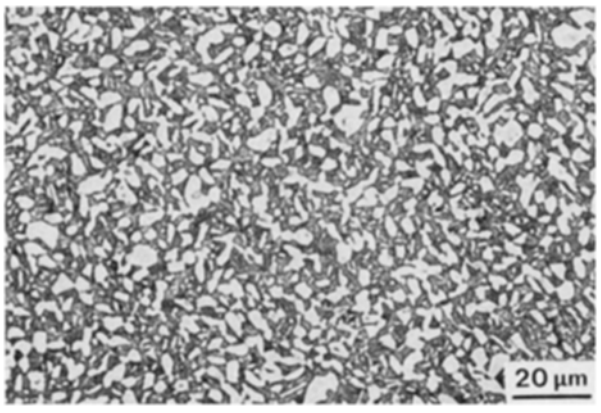


*Figure 1* $(\alpha + \beta)$ as-rolled and air-cooled microstructure. $D_\alpha = 2.6\,\mu m$, $V_\beta = 43\%$.

rolling temperature. This provided specimens with markedly different starting microstructures for the subsequent superplastic tensile experiments; a fine grained equiaxed $(\alpha + \beta)$ grain structure (Fig. 1) and a transformed $\beta$ grain structure (Fig. 2). These microstructures may be regarded as characteristic of those which would be encountered in hot-rolled sheet material and the welded regions in sheet material, respectively, and represent opposite limits in the microstructural requirements for the development of superplastic flow.

In addition, some of the $(\alpha + \beta)$ rolled material was annealed at 900 and 800° C and air cooled in order to equilibrate the $\alpha$- and $\beta$-phases at different $\alpha/\beta$ volume fractions and to simulate possible commercial annealing heat treatments. The microstructures are shown in Figs. 3 and 4, respectively. It can be seen that the 900° C anneal has resulted in a coarser $(\alpha + \beta)$ grain structure and a slight increase in $V_\beta$, the volume fraction of the $\beta$-phase (Fig. 3) and that the 800° C anneal has resulted in a limited amount of grain coarsening and a marked decrease in $V_\beta$ (Fig. 4). These results indicate that the temperature during the final states of rolling was slightly below 900° C. The very different etching response (in the standard 95 parts $H_2O$, 3 parts $HNO_3$, 2 parts HF solution) of the as-rolled and annealed microstructures should also be noted. In both Figs. 1 and 3 the $\beta$-phase has partially transformed to a network of $\alpha$ platelets (and should therefore strictly be designated "transformed $\beta$" at room temperature),

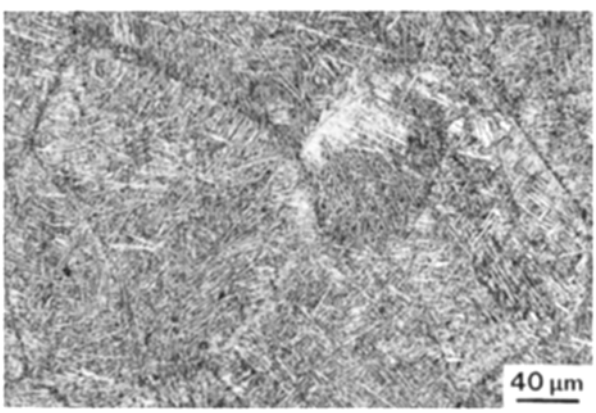


*Figure 2* $\beta$ as-rolled and air-cooled microstructure.

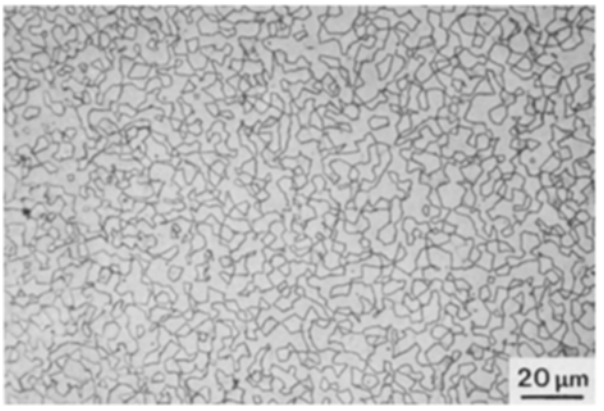


*Figure 3* As Fig. 1, followed by an anneal at 900° C for 24 h. $D_\alpha = 4.3\,\mu m$, $V_\beta = 51\%$.

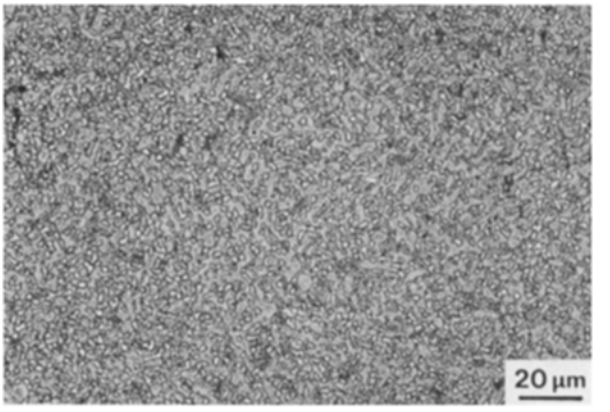


*Figure 4* As Fig. 1, followed by an anneal at 800° C for 16 h. $D_\alpha = 2.6\,\mu m$, $V_\beta = 38\%$.

but the finer scale of the platelets in the annealed material has, unlike the as-rolled material, resulted in an etching response very similar to that of the α-phase.

Round tensile specimens, 6.4 mm diameter and 20 mm gauge length, were machined from the bar material. High-temperature tensile experiments between 915 and 805° C were carried out using an Instron machine on to which was fitted a Mayes three-zone furnace which provided a 300 mm long uniform temperature hot zone accurate to ± 2° C. Crosshead speed cycling experiments were carried out in order to generate stress–strain rate data and crosshead reversal experiments were carried out in order to determine the internal stress, $\sigma_i$, as a function of strain rate. The following experimental procedure was adopted:

(i) equilibrate specimen at the testing temperature for 1 h;

(ii) strain the specimen an initial ~5% at a high crosshead speed of 2 mm $min^{-1}$ (corresponding to a strain rate of $\sim 1.67 \times 10^{-3}\,sec^{-1}$) and then reduce the crosshead to give the lowest strain rate;

(iii) crosshead speed cycle in (a minimum of) eight steps, corresponding to strain rates in the range $\sim 1.4 \times 10^{-5}$ to $\sim 3.5 \times 10^{-3}\,sec^{-1}$ in the strain range 0 to 20% and reduce the crosshead speed back to give the minimum strain rate;

(iv) repeat (iii), i.e. a second strain rate cycle in the strain range 20 to 40%;

(v) repeat (iii), except that at each crosshead speed step carry out crosshead speed reversal tests in order to determine $\sigma_i$; i.e. a third strain rate cycle in an extended strain range of 40 to 100%.

The tensile tests were not, in general, continued above about 100% strain (a) in order to provide specimens of sufficient diameter to prepare 3 mm discs for electron microscopy, and (b) because at higher strains non-uniformity of the strain in the gauge length renders the stress–strain rate data increasingly unreliable. However, several tests were carried out in order to demonstrate the maximum elongations which could be achieved in this alloy and typical examples are shown in Fig. 5. The crosshead speeds used in these experiments were chosen to correspond to strain rates close to those for maximum values of $m$ (see below).

The experimental load/crosshead speed/time data were plotted as log $\sigma$ against log $\dot{\varepsilon}$ data and a curve-fitting computer program using an equation of the form

$$\sigma = A + B(\log \dot{\varepsilon} \times 10^7)^C \qquad (1)$$

was used (a) to draw a smooth curve through the data points, and (b) to generate corresponding $m$ against log $\dot{\varepsilon}$ plots from the slope of the curve. $A$, $B$ and $C$ in the above equation are curve-fitting constants. A curve fitting accuracy analysis was carried out on each set of data in order to determine the correlation coefficients, average coefficients, standard deviations and deviation coefficients (measures of the accuracy of the curve-fitting procedures and deviation of individual data points from the curves). Typical values are given in Table I and indicate that both the curve-fitting procedure and the accuracy of the data points are excellent. The log $\sigma_i$ against log $\dot{\varepsilon}$ data were fitted to an equation of the form

$$\sigma_i = D\dot{\varepsilon}^F \qquad (2)$$

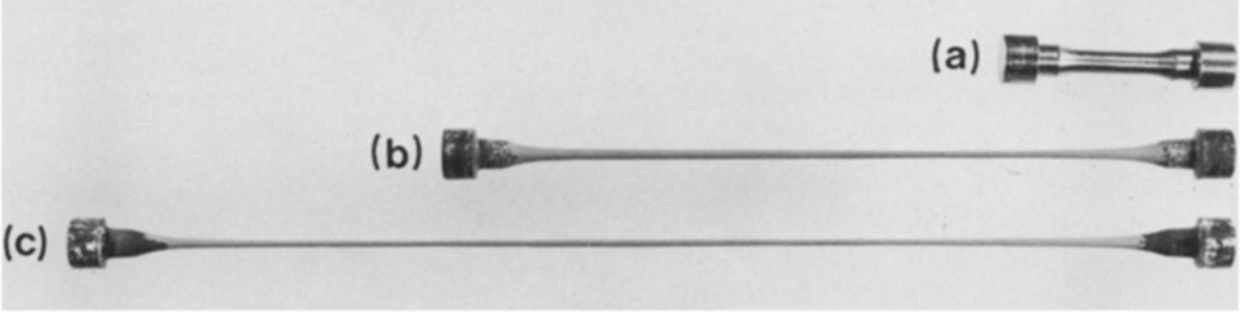


*Figure 5* Tensile specimens of (α + β) rolled alloy showing (a) undeformed test-piece, (b) elongations obtained at 880° C to 775%, and (c) 915° C to 1230%.

TABLE I Curve-fitting parameters for ($\alpha + \beta$) rolled material 915 to 805° C

| Test temp (° C) | Test cycle no. | Average (Av)* | Standard deviation (S.D.)† | Deviation coefficient (DC)‡ | Correlation coefficient (CC)§ | $A = \sigma_0$ (MPa) (Method c) | $B$ (MPa) | $C$ | $\sigma_{io}$ (MPa) (Method b) |
|---|---|---|---|---|---|---|---|---|---|
| 915 | 1 | 1.000 | 0.033 | 3,330 | 0.999 | 1.7200 | 0.0008 | 7.2128 | |
| | 2 | 1.000 | 0.069 | 6.925 | 0.994 | 1.8500 | 0.0041 | 6.1457 | |
| | 3 | 1.000 | 0.057 | 5.703 | 0.998 | 2.2200 | 0.0040 | 6.3169 | 1.65 |
| 880 | 1 | 1.000 | 0.083 | 8.317 | 0.991 | 3.2450 | 0.0032 | 6.5835 | |
| | 2 | 1.000 | 0.029 | 2.884 | 0.998 | 2.9800 | 0.0123 | 5.7444 | |
| | 3 | 1.001 | 0.036 | 3.576 | 0.996 | 1.9450 | 0.0400 | 5.0280 | 1.80 |
| 850 | 1 | 1.000 | 0.020 | 1.952 | 0.999 | 3.5600 | 0.1545 | 4.1017 | |
| | 2 | 1.000 | 0.044 | 4.417 | 0.999 | 5.1450 | 0.0839 | 4.5444 | |
| | 3 | 1.002 | 0.034 | 3.353 | 0.999 | 4.9450 | 0.0903 | 4.4683 | 4.90 |
| 805 | 1 | 1.000 | 0.069 | 6.923 | 0.995 | 14.3100 | 0.2064 | 4.2243 | |
| | 2 | 1.000 | 0.034 | 3.387 | 0.998 | 12.3700 | 0.3460 | 3.9013 | |
| | 3 | 1.000 | 0.032 | 3.167 | 0.998 | 8.4100 | 0.1844 | 4.2505 | 10.10 |

*Av $= \frac{1}{N}\Sigma\left(\frac{\sigma_t}{\sigma_e}\right)$, where $N$ is the number of experimental flow stress measurements over strain rate range, $\sigma_e$ the experimental flow stress, and $\sigma_t$ the corresponding flow stress given by Equation 1.

†S.D. $= \left[\frac{1}{N}\Sigma\left(\frac{\sigma_e}{\sigma_t} - 1\right)^2\right]^{1/2}$

‡DC $= \frac{\text{SD}}{\text{Av}} \times 100\%$.

§CC $= \left\{1 - \frac{\Sigma(\sigma_t - \sigma_e)^2}{\Sigma[\sigma_e - (\Sigma\sigma_e/N)]^2}\right\}^{1/2}$.

where $D$ and $F$ are curve-fitting constants and $F$ expresses the uniform slope of the log $\sigma_i$ against log $\dot{\varepsilon}$ data.

The threshold stress, $\sigma_0$, which is defined as the stress below which deformation will not occur, may be estimated in three ways

1. by an extrapolation of the stress–strain rate data (plotted on linear scales) to zero strain rate. This is not a very satisfactory procedure because the extrapolation has usually to be carried out over a large strain rate range and is usually assumed to be linear – an assumption which implies that the strain rate sensitivity in the extrapolation range is unity;
2. by extrapolating the log $\sigma_i$ against log $\dot{\varepsilon}$ data as described by Equation 2 to a very low strain rate, e.g. at $10^{-7}\,\text{sec}^{-1}$, $\sigma_i \rightarrow \sigma_{io}$;
3. by identifying $\sigma_0$ with $A$, one of the constants in the curve-fitting Equation 1 above. This is also an extrapolation procedure but it is more satisfactory than method 1 insofar as it is not linear and its accuracy can also be assessed from the extent to which Equation 1 accurately describes the experimental data.

The values of the threshhold stresses determined by methods 2 and 3 above, the values of the curve fitting constants $A$, $B$, $C$ (Equation 1) and the parameters which define the accuracy of the curve fitting procedure and the scatter in the experimental data points from the curve, are given in Table I.

Longitudinal and transverse sections from the gauge lengths of the deformed specimens were prepared for light, scanning and 200 kV transmission electron microscopy in the usual way. Energy dispersive X-ray analysis was carried out on longitudinal SEM and TEM specimens, using the SEM at an operating potential of 20 kV.

## 3. Results

The superplastic properties of IMI550 in all four microstructural conditions (Figs. 1 to 4) were measured at 915 and 850° C. The stress–strain rate and derived strain rate sensitivity data at 915° C for the ($\alpha + \beta$) and $\beta$ rolled material are shown in Figs. 6 and 7 and the microstructures after 100% superplastic strain are shown in Figs. 8 and 9, respectively. In the ($\alpha + \beta$) rolled material, the flow stresses *increase* with strain (as shown by the data for the first, second and third strain rate cycles) (Fig. 6a). This indicates concurrent grain coarsening, as is indeed shown to be the case by a comparison of Figs. 1 and 8. On the other hand, in the $\beta$ rolled material the flow stresses *decrease* with strain, indicating a break-up of the acicular $\alpha$ (transformed $\beta$) grain structure. Again, a comparison of Figs. 2 and 9 shows this to be the case and, moreover, that the microstructures which, prior to the superplastic deformation were very different (Figs. 1 and 2), are now converging or becoming similar with respect both to grain size, shape and $\alpha/\beta$ volume fraction. The flow stresses are also converging (compare Figs. 6 and 7) which suggests that at this temperature there exists an equilibrium grain size for strain rate cycled material. Also included in Fig. 6 are the data for the material annealed at 900° C (dashed line). Again, the coarser initial grain size following this annealing treatment (Fig. 3) has resulted, in general, in higher flow stresses. The data for the 800° C annealed material is not included in Fig. 6; it coincides very closely with that of the as-rolled material as indeed is expected from the lack of grain coarsening at this annealing temperature (Fig. 4).

The corresponding stress–strain rate and derived strain rate sensitivity data at the lower temperature of 850° C are shown in Figs. 10 and 11 and examples of the microstructures after 100% strain are shown in

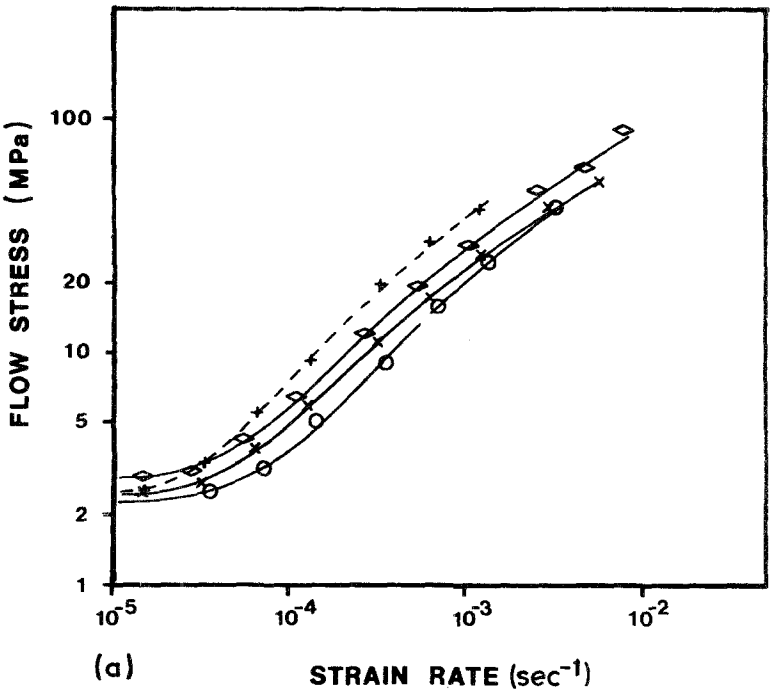


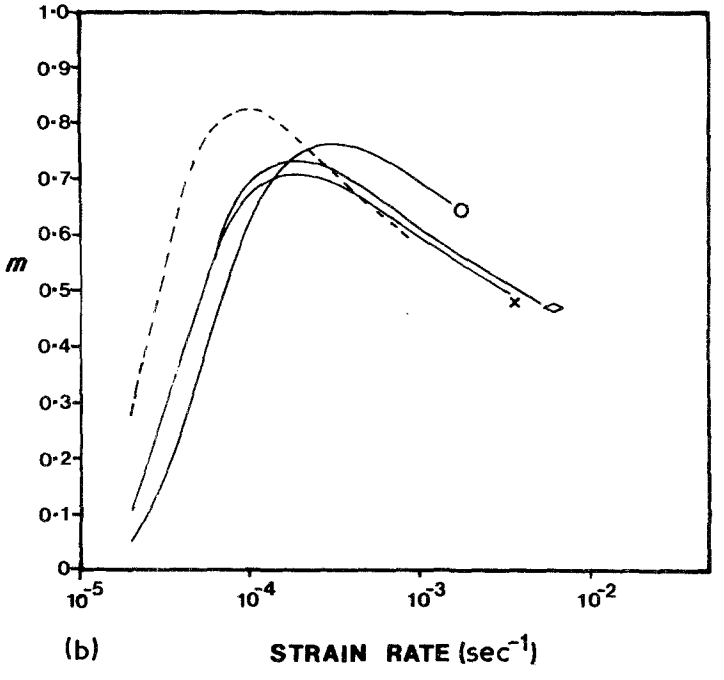


*Figure 6* (a) Log $\sigma$ against log $\dot{\varepsilon}$ and (b) $m$ against log $\dot{\varepsilon}$ plots for ($\alpha$ + $\beta$) rolled material at 915° C (———), showing strain-dependent flow stresses arising from grain coarsening. Cycles (○) 1, (×) 2 and (◆) 3 correspond to the approximate strain ranges 5 to 20%; 20 to 40%; 40 to 100%. The plot for cycle 2 for the material annealed at 900° C is also included (dashed curve).

Figs. 12 and 13. For the ($\alpha$ + $\beta$) rolled material (Fig. 10), the flow stresses are almost strain-independent (except for small decreases in flow stresses with increasing strain at the lower strain rates) which indicates negligible grain coarsening. The microstructures of the material deformed at this temperature showed this to be the case. Fig. 10 also includes the data for the material annealed at 900° C (dashed curve). Again, the higher flow stresses result from the coarser initial grain size (Fig. 3) and grain coarsening during superplastic testing at 850° C was not observed. Rather, a slight refinement of the grain structure occurred as may be seen by a comparison of Fig. 12, showing the material at 100% strain, and Fig. 3, the initial annealed microstructure. The data for the material at 800° C again coincided very closely with that for the as-rolled material and are not included.

The results for the $\beta$ rolled material (Fig. 11) follow the same pattern as those at 915° C (Fig. 7); i.e. reduced flow stresses with increasing strain and an associated break-up and refinement of the acicular $\alpha$ microstructure (Fig. 13). Furthermore, the strain rate sensitivity increases with strain (Fig. 11b) such that, during deformation, the material moves from a non-superplastic to a superplastic condition.

The internal stresses, $\sigma_i$, as a function of strain rate for the ($\alpha$ + $\beta$) and $\beta$ rolled material at 915 and 850° C are shown in Figs. 14 and 15, respectively. The testing procedure (see above) did not allow measurements of $\sigma_i$ to be made as a function of strain and these data correspond to the third strain rate cycle. Four points should be noted: (i) the $\sigma_i$ values increase slightly with strain rate; (ii) they are greater for the $\beta$ rolled than the $\alpha$ + $\beta$ rolled material; (iii) they decrease with increase in temperature; and (iv) the differences between the $\sigma_i$ values for ($\alpha$ + $\beta$) and $\beta$ rolled material

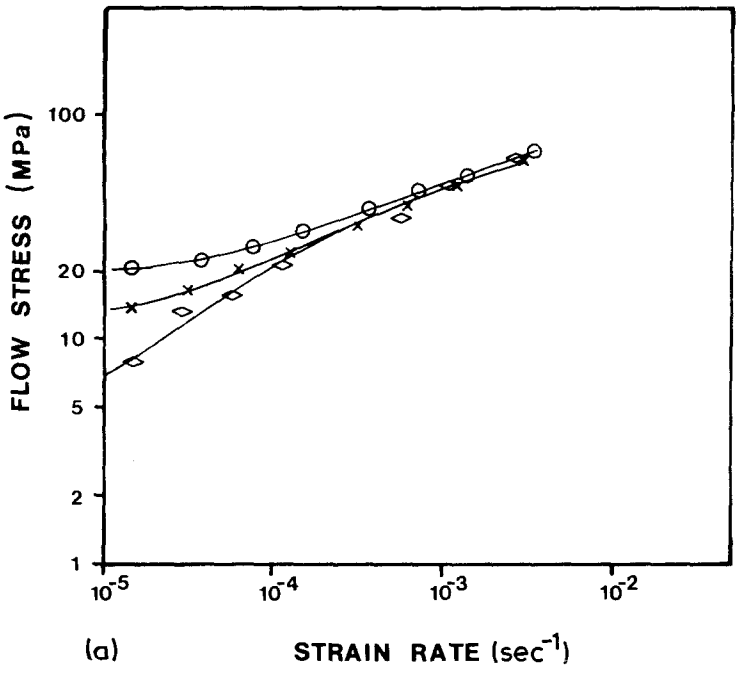


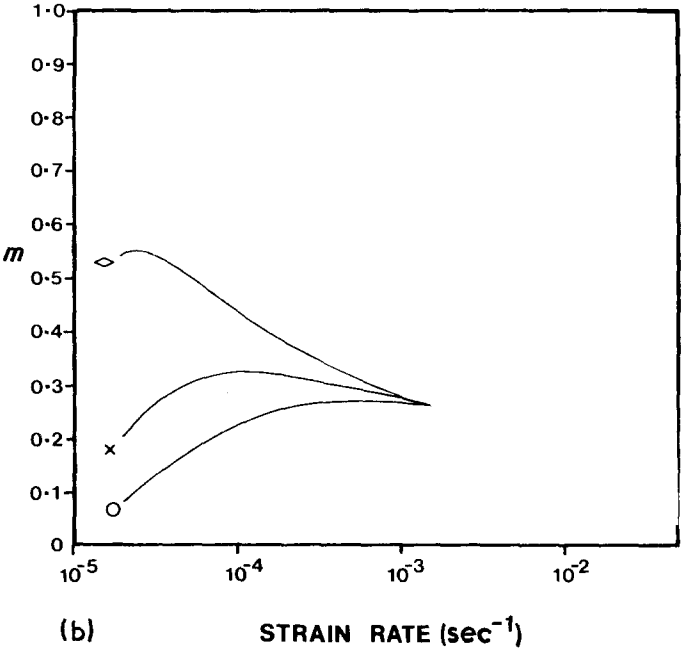


*Figure 7* (a) Log $\sigma$ against log $\dot{\varepsilon}$ and (b) $m$ against log $\dot{\varepsilon}$ plots for $\beta$ rolled material at 915° C (———), showing strain-dependent flow stresses arising from grain refinement. Strain ranges for cycles (○) 1, (×) 2 and (◇) 3 as for Fig. 6.

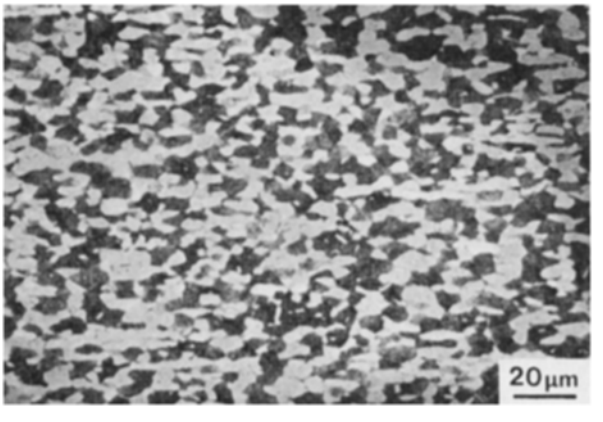


*Figure 8* As Fig. 1, followed by superplastic tensile testing at 915° C to ~ 100% strain. Longitudinal section showing coarsening of the $\alpha + \beta$ microstructure ($D_\alpha$ = 2.8 $\mu$m).

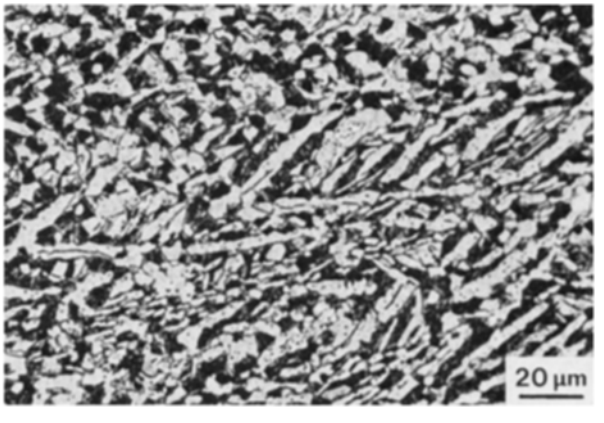


*Figure 9* As Fig. 2, followed by superplastic tensile testing at 915° C to ~ 100% strain. Longitudinal section showing break-up of the acicular $\alpha$/transformed $\beta$ microstructure.

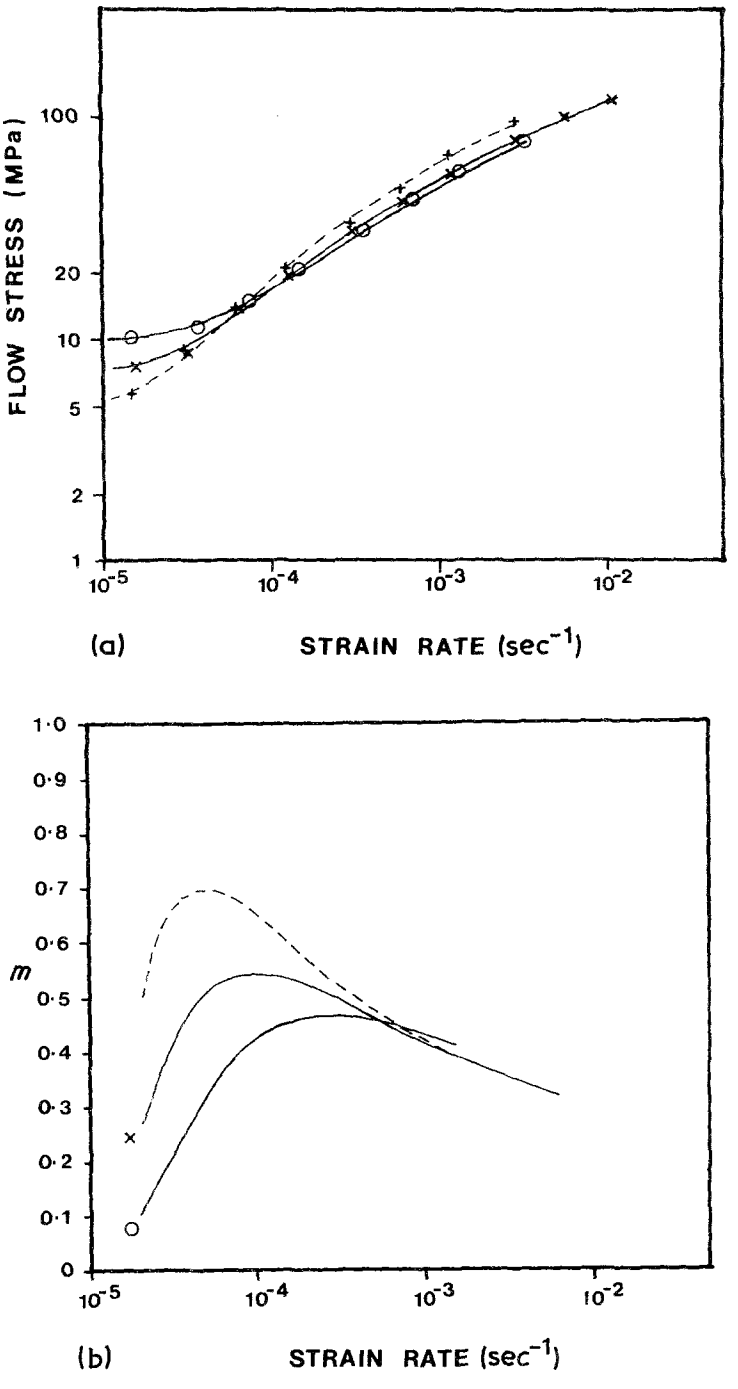


*Figure 10* (a) Log $\sigma$ against log $\dot{\varepsilon}$ and (b) $m$ against log $\dot{\varepsilon}$ plots for ($\alpha$ + $\beta$) rolled material at 850° C (———), showing approximate strain-independent flow stresses (cycle 2 up to 40% strain). The plot for cycle 2 for the material annealed at 900° C is also included (dashed curve). (○) Cycle 1, (×) Cycle 2.

are insufficient to account for the differences between the flow stresses for these two microstructural conditions; i.e. the "reduced" flow stress (log ($\sigma$–$\sigma_i$)) against strain rate data are not microstructure independent.

The stress–strain rate results for ($\alpha$ + $\beta$) rolled material for a range of temperatures between 915 and 805° C are shown in Fig. 16a. These data refer to the second strain rate cycle (i.e. strains between 20 and 40%). It is considered that these are most representative of the properties of the typical equiaxed ($\alpha$ + $\beta$) microstructures in IMI550 as shown in Fig. 1, because (a) only moderate (if any) grain coarsening will have occurred, and (b) any transient effects at low strains will have been eliminated. The derived strain rate sensitivity plots are shown in Fig. 16b and show that only at the lowest temperature (805° C) does the material not attain a superplastic condition. The corresponding microstructure after ~100% strain shows clearly elongated ($\alpha$ + $\beta$) grains (Fig. 17).

The "reduced" flow stress, i.e. ($\sigma$ – $\sigma_i$) against strain rate curves at 915, 850 and 805° C are shown in Fig. 18. These data clearly show that, except at the lowest temperature where the material does not achieve a superplastic condition, the measured internal stress is able to account for the sigmoidal shape of the stress–strain curves: i.e. the strain rate sensitivity continues to increase with decreasing strain rate to the value of unity predicted by the diffusional creep mechanisms.

Light microscopy indicates that in the ($\alpha$ + $\beta$) rolled material the $\beta$-phase is the continuous or near-continuous phase (i.e. there is greater connectivity between the $\beta$ grains in the microstructure) even when the volume fraction of $\beta$ is less than that of $\alpha$. This can be seen by comparing the optical micrographs of the

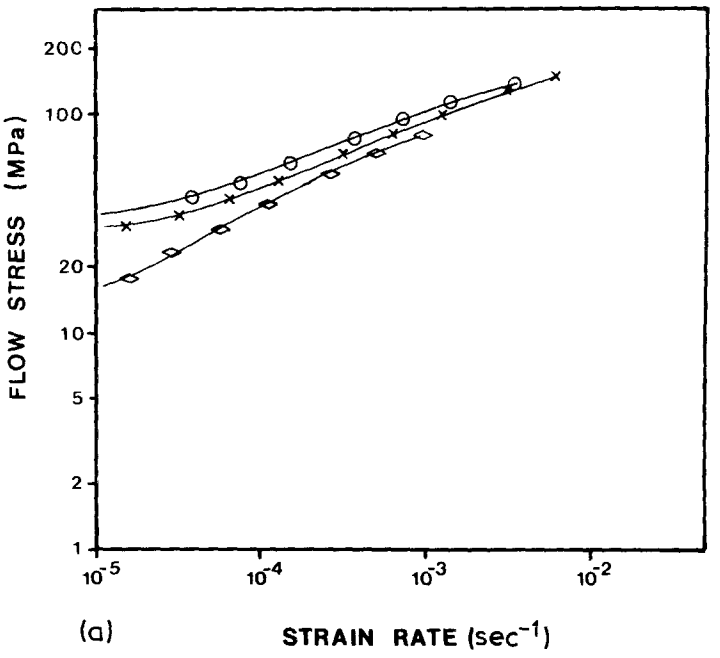


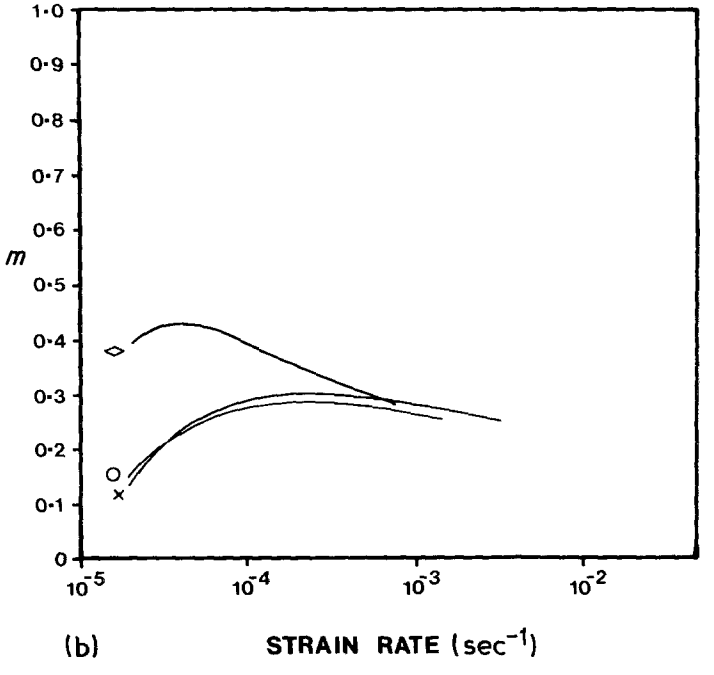


*Figure 11* (a) Log $\sigma$ against log $\dot{\varepsilon}$ and (b) $m$ against log $\dot{\varepsilon}$ plots for $\beta$ rolled material at 850° C (———) showing strain-dependent flow stresses arising from grain refinement. (Cycle 3 up to ~100% strain). (○) Cycle 1, (×) Cycle 2, (◇) Cycle 3.

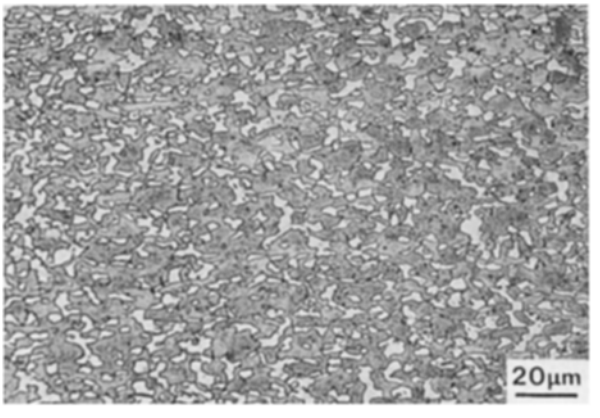


*Figure 12* As Fig. 3, followed by superplastic tensile testing at 850° C to ~100% strain. Longitudinal section showing slight refinement of ($\alpha$ + $\beta$) microstructure ($D_\alpha$ = 3.8 $\mu$m) as compared to Fig. 3.

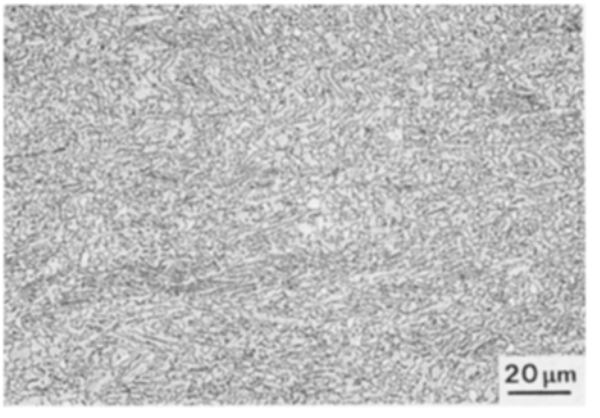


*Figure 13* As Fig. 2, followed by superplastic tensile testing at 850° C to ~100% strain. Longitudinal section showing a microstructure intermediate between an acicular $\alpha$ and equiaxed ($\alpha$ + $\beta$).

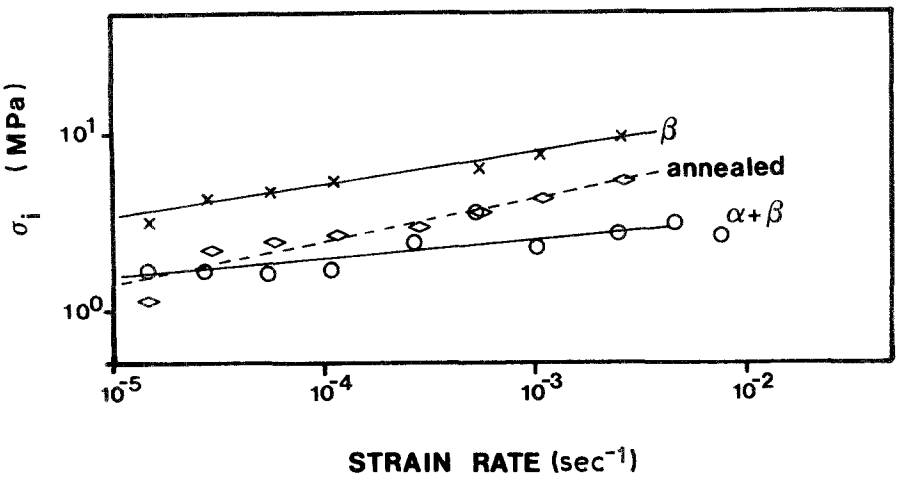


*Figure 14* Log $\sigma_i$ against log $\dot{\varepsilon}$ plots for ($\alpha + \beta$) and $\beta$ rolled material and 900° C annealed material at 915° C.

specimens superplastically deformed at 915° C (Fig. 8) and 850° C (Fig. 12). The $\alpha/\beta$ interphase boundaries are curved convex towards the $\beta$-phase such that at triple points the interphase boundaries tend to make an acute angle across the $\beta$-phase; the $\beta$-phase therefore in effect wets the $\alpha/\beta$ grain boundaries in accordance with the behaviour predicted by Springarn and Nix [14].

The connectivity of the $\beta$-phase is more clearly revealed in the scanning electron micrographs (Fig. 19). EDAX measurements were taken in the centres of $\beta$ grains and close to the longitudinal and transverse interphase boundaries (with respect to the tensile axis) in order to detect any molybdenum segregation. The results obtained by a simple comparison of Mo$L\alpha$ peak intensities and upon which no ZAF corrections have been made are shown in Table II and examples of the SEM and TEM data for variation in Mo$L\alpha$ peak intensity between the centre, transverse and longitudinal boundaries of a grain given in Figs. 20 to 22. These data clearly show strong segregation of molybdenum at the longitudinal boundaries (in accordance with its slower diffusional properties) and (because of the much greater variations in Mo$L\alpha$ intensities in the TEM data, Figs. 21 and 22) the necessity of ZAF correction procedures to the SEM data (Fig. 20). This variation in molybdenum content within the $\beta$ grains would be expected to give rise to a corresponding variation in the $\beta$ transformation behaviour upon cooling down to room temperature, but no variation in the extent of the transformation and scale and distribution of the $\alpha$ platelets within the $\beta$ grains was detected.

## 4. Discussion

The results show that IMI550 with an ($\alpha + \beta$) microstructure and a grain size of $\sim 3\,\mu m$ exhibits superplasticity (i.e. strain rate sensitivities $> 0.4$) for limited strain rate ranges at temperatures down to 850° C (Fig. 16b). The superplasticity is strain-dependent, or more strictly time-dependent because of concurrent grain growth. This effect is only marked, however, at the higher temperatures and it is a fortunate circumstance that at lower temperatures where the extent of superplasticity is more limited, the loss of superplasticity arising from grain growth is negligible. The results also show that superplasticity is a deformation property which is dependent upon, and may develop as a result of, the method of strain rate cycling as employed in this and most previous works. In particular, the break-up and development of fine equiaxed ($\alpha + \beta$) microstructures from the transformed microstructures characteristic of $\beta$ forged material can only occur if the strain rate cycling is partially carried out in strain rate regimes where the deformation is primarily accommodated by dislocation climb-controlled creep processes (i.e. Region III). Otherwise it is difficult to see how diffusional creep, which forms the basis of all superplastic deformation mechanisms, irrespective of the particular proposed diffusional

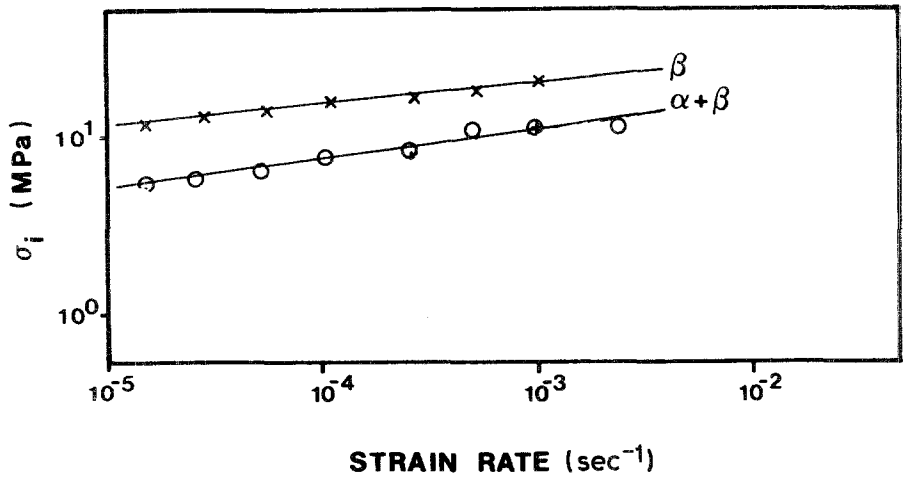


*Figure 15* Log $\sigma_i$ against log $\dot{\varepsilon}$ plots for ($\alpha + \beta$) and $\beta$ rolled material at 850° C.

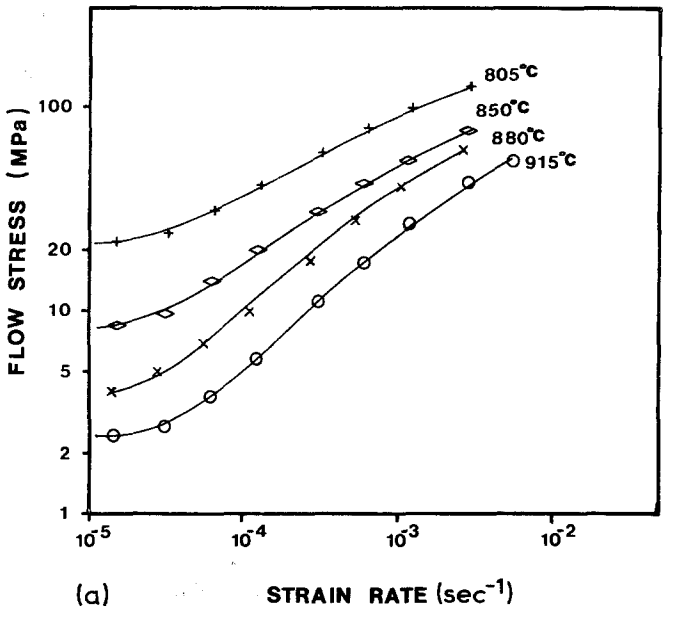


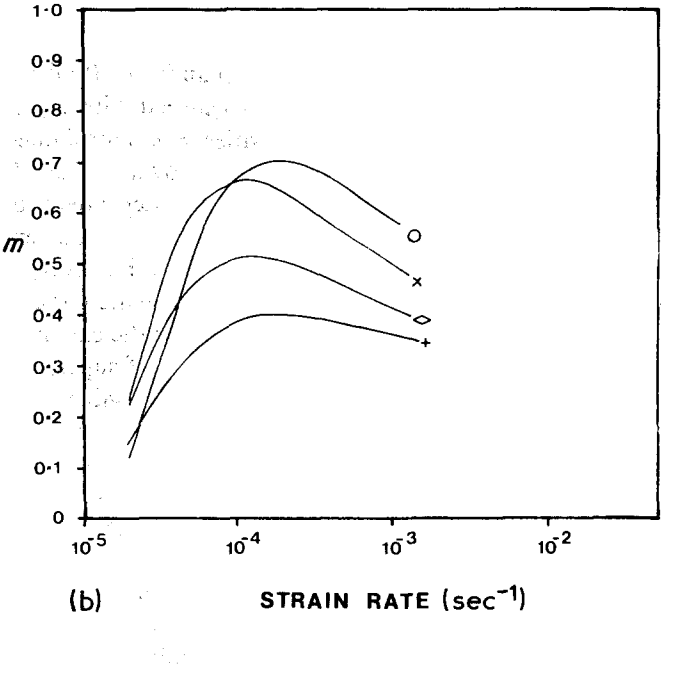


*Figure 16* (a) Log $\sigma$ against log $\dot{\varepsilon}$ and (b) $m$ against log $\dot{\varepsilon}$ data for ($\alpha + \beta$) rolled material for temperature range 805 to 915° C (second cycle, strain range 20 to 40%).

paths and geometry of grain translations, can give rise to a refinement of the microstructure. The development of superplasticity in the $\beta$ forged material in this work is therefore a consequence of the method of strain rate cycling. However, it is also true that, as deformation proceeds and the microstructure is refined, the transition from predominantly dislocation climb-controlled creep to diffusional-controlled creep (i.e. the transition from Region III to Region II) occurs at increasing strain rates. It is therefore possible that superplasticity may be developed in transformed $\beta$ microstructures during constant strain rate tests in which the strain rate corresponds to Region III for the initial microstructure but to Region II for the refined microstructure. Such appears to be the case from the work of Cope [21] who carried out constant strain rate tests in Ti–6% Al–4% V tensile specimens containing welds which exhibit transformed $\beta$ microstructures analogous to those resulting from $\beta$ forging.

TABLE II Segregation ($S$) of molybdenum between longitudinal (l) and transverse (t) $\beta$ grain boundaries. $S = (I_l - I_t)/I_t$ where $I$ = intensity of Mo$L\alpha$

| Method | Measurements on different $\beta$ grains | Average $S$ |
|---|---|---|
| SEM (20 kV) | 0.34, 0.32, 0.30, 0.30, 0.35 | 0.32 |
| TEM (200 kV) | 2.2, 3.9, 2.8, 3.1, 2.8 | 3.0 |

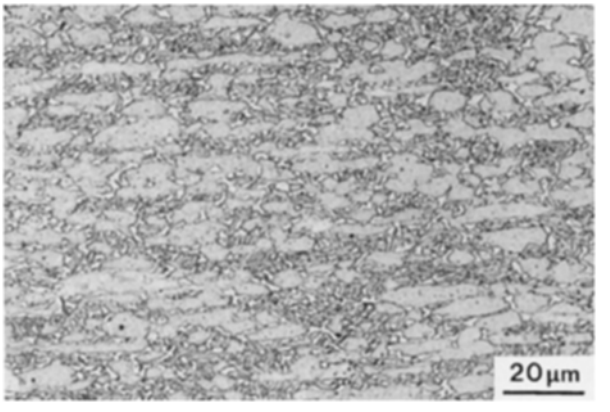


*Figure 17* As Fig. 1, followed by ~ 100% strain at 805° C showing elongated microstructure not characteristic of superplastic deformation.

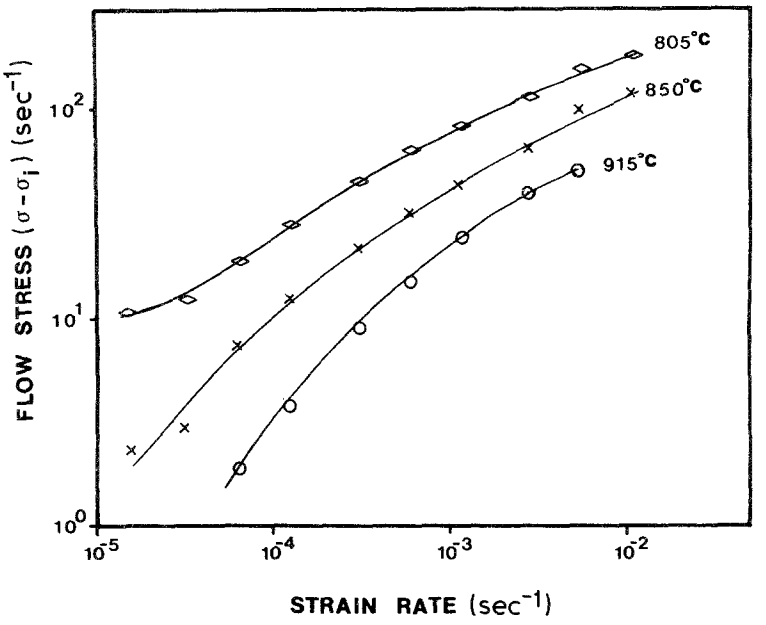


*Figure 18* Log ($\sigma - \sigma_i$) against log $\dot{\varepsilon}$ data for ($\alpha + \beta$) rolled material at 915, 850 and 805° C.

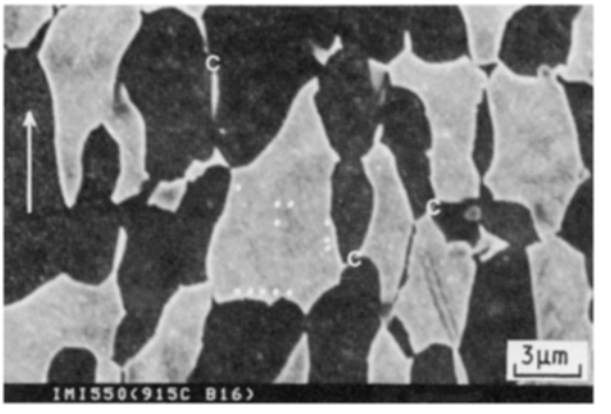


*Figure 19* Scanning electron micrograph of material superplastically deformed at 915° C showing curved interphase boundaries, connectivity of $\beta$-phase (indicated by C) and microanalysis positions within a $\beta$ grain (indicated by white dots). Tensile axis direction indicated by arrow.

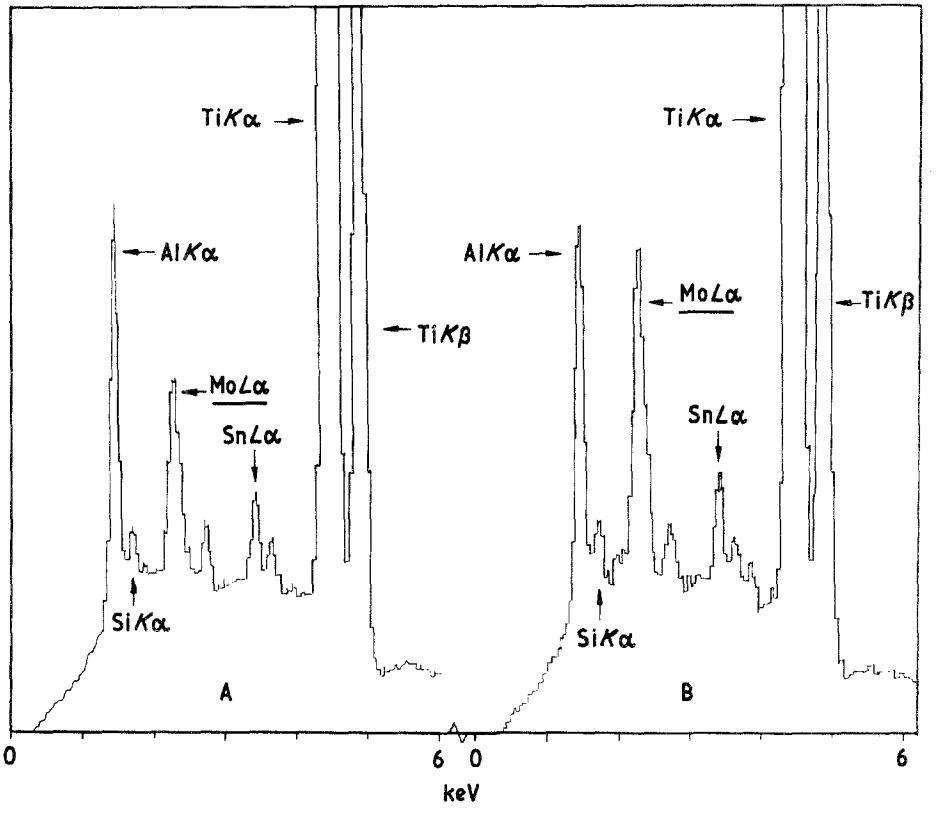


*Figure 20* Energy dispersive X-ray analysis data in the SEM showing increase in Mo$L\alpha$ intensity from the transverse interphase boundary (A) to the longitudinal boundary (B).

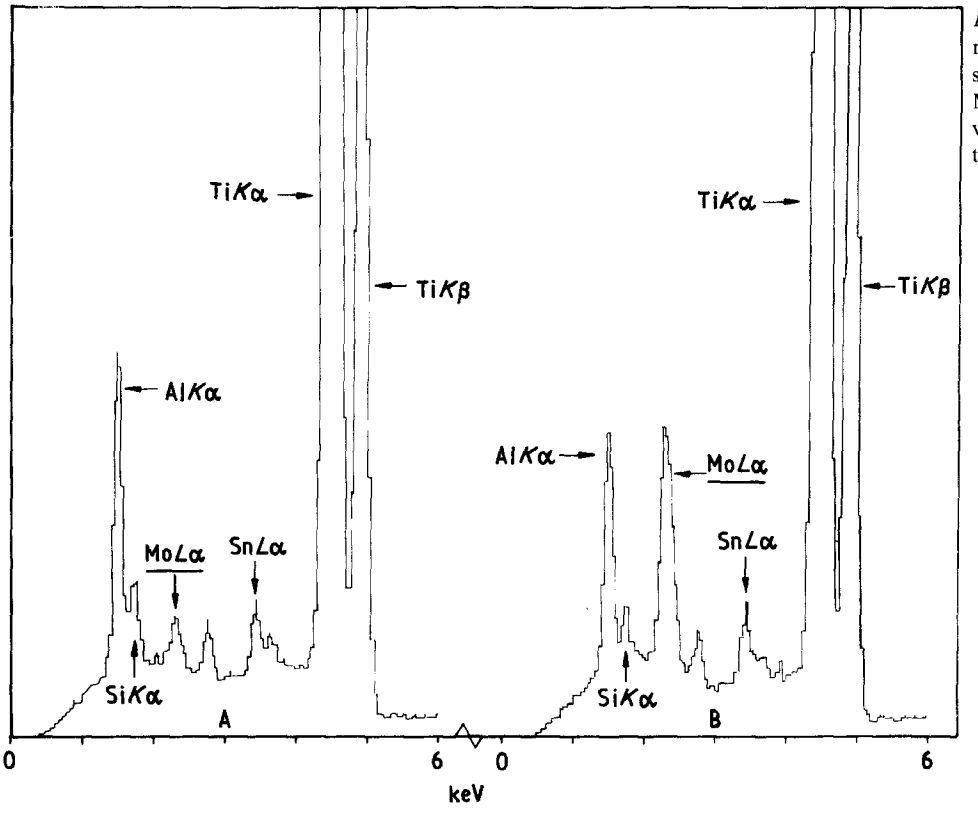


*Figure 21* Energy dispersive X-ray analysis data in the TEM showing marked increase in Mo$L\alpha$ intensity from the transverse interphase boundary (A) to the centre of the grain (B).

Again an equiaxed ($\alpha + \beta$) microstructue was developed during the deformation.

The present results also show that the transition from Region II to Region I, the sigmoidal shape of the stress–strain rate curves and the associated decrease in strain rate sensitivity can be accounted for on the basis of an internal stress $\sigma_i$. It is, however, not yet possible to satisfactorily account for the measured values of $\sigma_i$ (and their dependence upon microstructure, temperature and strain rate) in terms of the variation of grain volume (as in the simple grain-switching model of Ashby and Verrall [11]) or the energy barriers which may be required for the emission or absorption of vacancies at grain boundaries. The latter problem is particularly difficult in two-phase materials in which both grain ($\alpha/\alpha$ and $\beta/\beta$) and interphase ($\alpha/\beta$) boundaries must be considered. However, the metallographic evidence indicates that it is the $\alpha/\beta$ boundaries which are of importance since the $\beta$ becomes the continuous phase in the microstructure.

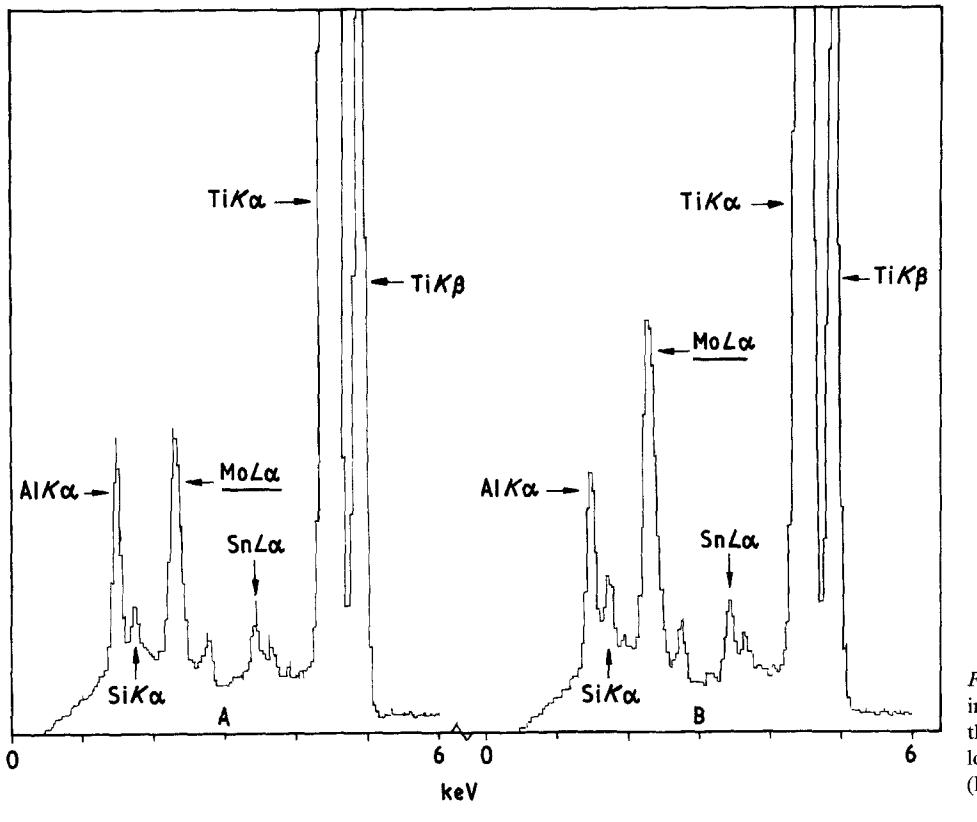


*Figure 22* As Fig. 21, showing increase in Mo$L\alpha$ intensity from the centre of the grain (A) to the longitudinal interphase boundary (B).

The $\beta$ phase becomes, to use Gifkins' terminology [13], the (deforming) mantle around the (relatively rigid) $\alpha$ grains. Furthermore, the strain and strain rate distribution between the $\alpha$-phases and $\beta$-phases which are a consequence of this mechanism, imply that it is the "isostress" model that provides a more adequate description of the overall superplastic behaviour.

The observed segregation of the slow-diffusing alloying element molybdenum at the longitudinal interphase boundaries of the $\beta$ grains corroborates previous work in which it was shown that fast-diffusing alloying elements segregate to the transverse boundaries [20]. Such variations in alloying element concentrations in the (relatively) equiaxed grains of Fig. 19 are in accordance with the occurrence of both Herring–Nabarro and Coble creep within the $\beta$ grains. Of more significance, however, is the alloying element concentration in the $\beta$ layers or mantle around the $\alpha$ grains. In previous work [20] it was suggested that it was the fast diffusing alloying elements which would become concentrated within these layers in accordance with the predictions of the model of Springarn and Nix [14]. Conversely, the slow diffusing alloying element, molybdenum, would be expected to become depleted within these layers. However, neither predictions have yet been confirmed by experiment because of the problem of carrying out satisfactory analyses in regions close to $\alpha/\beta$ interphase boundaries.

## Acknowledgements

The authors wish to thank Professor J. Nutting, Department of Metallurgy, University of Leeds, for the provision of laboratory facilities, and Mrs Joan Nathan for typing the manuscript.

## References

1. IMI Titanium 550 Data Sheet, IMI Titanium Ltd, PO Box 216, Birmingham 6, UK.
2. British Aerospace, Preston Division, private communication (1984).
3. D. LEE and W. A. BACKOFEN, *Trans. TMS-AIME* **239** (1967) 1034.
4. A. ARIELI and A. ROSEN, *Metall. Trans. A* **8A** (1977) 1591.
5. N. E. PATON and C. H. HAMILTON, *Metall. Trans.* **10A** (1979) 241.
6. A. K. GHOSH and C. H. HAMILTON, *ibid.* **10A** (1979) 699.
7. G. HILAIRE, E. BUDILLON, E. HUELLEC and J. CHANTERANNE, "Titanium '80", Proceedings of the 4th International Conference on Titanium, Kyoto (1980) (Metallurgical Society AIME, Warrendale, Pennsylvania, 1980) p. 1033.
8. T. ENJO, K. IKEUCHI, N. AIKAWA and M. ITO, *ibid.*, p. 1097.
9. C. W. CORTI and G. H. GESSINGER, "Forging and Properties of Aerospace Materials" (Metals Society, London, 1978) p. 266.
10. C. H. CHEN and J. E. COYNE, *Metall. Trans. A.* **7A** (1976) 1931.
11. M. F. ASHBY and R. A. VERRALL, *Acta Metall.* **21** (1973) 149.
12. E. ARZT, M. F. ASHBY and R. A. VERRALL, *ibid.* **31** (1983) 1977.
13. R. C. GIFKINS, *J. Mater. Sci.* **13** (1978) 1926.
14. J. R. SPRINGARN and W. D. NIX, *Acta Metall.* **26** (1978) 1389.
15. D. GRAHAM, "Diffusion in Body Centred Cubic Metals", Proceedings of the 4th International Conference on Diffusion in bcc Metals, Gatlinburg, Tennessee (1964) (ASM, Metals Park, Ohio, 1965) p. 27.
16. R. RAJ and A. K. GHOSH, *Acta Metall.* **29** (1981) 283.
17. A. K. GHOSH and R. RAJ, *ibid.* **29** (1981) 607.
18. J. R. LEADER, D. F. NEAL and C. HAMMOND, *Metall. trans. A.* in press.
19. J. WERT and N. E. PATON, *ibid.* **14A** (1983) 2535.
20. JIMIN MA and C. HAMMOND, Proceedings 5th International Conference on Titanium, Munich (1984) (Deutsche Gesellschaft für Metallkunde EV. Oberursel, 1985) p. 703.
21. M. T. COPE, PhD thesis, University of Manchester (1984).

*Received 19 February*
*and accepted 13 March 1985*